Polymer Bulletin (2024) 81:12013–12026
https://doi.org/10.1007/s00289-024-05254-5

ORIGINAL PAPER

Investigation of crystal habit of *N,N′*-dicyclohexylterephthalamide and its influence on the crystallization behavior of isotactic polypropylene

Jian Wang[1] · Guojun Luo[2] · Yanhua Niu[1] · Guangxian Li[1]

Received: 1 September 2023 / Revised: 25 January 2024 / Accepted: 3 April 2024 /
Published online: 4 May 2024

Abstract

In this paper, the *N,N′*-dicyclohexylterephthalamide (DCHT) with various morphologies and sizes was prepared by antisolvent precipitation at room temperature, and DCHT single crystals were also grown. Among them, DCHT crystals precipitated from deionized water (H_2O), alcohol (C_2H_5OH) and *N′N*-dimethylformamide (DMF) are particle-like crystallites (DCHT-H_2O), cuboid (DCHT-C_2H_5OH) and large rectangular crystals (DCHT-DMF), respectively. The powder XRD results show that the (002) plane is the dominant growth plane of the DCHT crystals, and the diffraction peak intensity of (100) plane is negatively correlated with the size of the DCHT crystals. The single-crystal XRD results show that the minimum distance between the two nearest DCHT molecules is the hydrogen bond distance (2.21 Å), and the (100) crystal plane is the plane of hydrogen bonding between DCHT molecules. Thus, it is speculated that the hydrogen bonding interaction is the main driving force for the growth of DCHT crystals. Further, the effect of different morphologies and sizes of DCHT on isotactic polypropylene (*i*PP) crystallization was investigated. Non-isothermal crystallization studies revealed that the DCHT size plays a decisive role in increasing the crystallization temperature of *i*PP. Through isothermal crystallization, it was found that the upper critical temperature of β-α growth "transition" of *i*PP could be related to the morphology of DCHT. Finally, the *i*PP film was attached to the surface of DCHT single crystal, and its crystallization behavior was studied. It is confirmed that the (001) plane is the epitaxial plane of DCHT to the β-*i*PP molecular chain, while the epitaxial plane of β-*i*PP is the (110) plane.

✉ Yanhua Niu
yhniu@scu.edu.cn

✉ Guangxian Li
guangxianli@scu.edu.cn

[1] College of Polymer Science and Engineering, State Key Laboratory of Polymer Materials Engineering of China, Sichuan University, Chengdu 610065, China

[2] KingFa Science and Technology Co. Ltd., Guangzhou 510663, China

Keywords Isotactic polypropylene · Nucleator · Epitaxial crystallization

Introduction

The semicrystalline polymer isotactic polypropylene (*i*PP) has been widely used in many fields due to its advantageous properties and low cost. However, specific practical applications of *i*PP often require enhancements in optical transparency, mechanical properties and heat resistance, as well as a reduction in processing cycle time. The slow crystallization rate of *i*PP limits its applications, necessitating the introduction of nucleating agents (NAs) to enhance its crystallization properties during processing. It is reported that not only the crystallization capacity, but also the crystal transformation and crystal morphology could be affected by NA [1–3]. As we know, *i*PP can crystallize into several forms, including monoclinic α, trigonal β and orthorhombic γ [4–8]. Notably, β crystals, induced by β NAs, confer enhanced mechanical properties to *i*PP, garnering significant interest.

So far, there have been a lot of reports on the synthesis of β NAs and its inducing mechanism of β-*i*PP. Schmidt's group synthesized a series of amide NAs and investigated their effects on the crystallization behavior of *i*PP in detail [6]. Among them, *N*,*N'*-dicyclohexylterephthalamide (DCHT) exhibits the best nucleation performance and shows various self-assembled structures under different temperature and shear conditions [9–11]. Feng et al. [12, 13] found that the self-assembled structure of DCHT is mainly determined by the degree of dissociation of DCHT molecules and the dispersion state in the melt. In addition, *i*PP crystallization induced by DCHT belongs to epitaxial crystallization [14–16], which requires lattice matching. Lotz et al. [17] confirmed that the epitaxial lattice of DCHT exhibits a periodicity of 6.5 Å, and identifying that the (110) crystal plane of β-*i*PP is its epitaxial plane. Wang et al. [18] prepared DCHT single crystals by solution method and determined the cell parameters of DCHT by single-crystal X-ray diffraction (XRD). To sum up, the regulation of self-assembled structures of DCHT are mainly achieved by changing the final heating temperature (T_f), concentration and shear field, which could further significantly influence the crystallization of *i*PP. However, most current studies used commercial DCHT and the effect its original crystal morphology on the *i*PP crystallization are neglected.

In this work, the crystal habit of DCHT was regulated by antisolvent precipitation method [19–23]. Some solvents that are common and have very low DCHT solubility are selected as antisolvents, including deionized water (H_2O), ethyl alcohol (C_2H_5OH) and *N'N*-dimethylformamide (DMF). The commercial DCHT was initially dissolved in sulfuric acid (H_2SO_4), and then, the solution was pulled into various antisolvents, through which the DCHT crystals with various morphologies were obtained. The crystal habits of DCHT in different antisolvents was elucidated by XRD and scanning electron microscope (SEM). The results show that the hydrogen bond interaction could be the main driving force of DCHT crystal growth. Furthermore, the effect of DCHT crystals with different morphologies and sizes on the crystallization of *i*PP was investigated. Finally, *i*PP film was attached to the surface of DCHT single crystals and the epitaxial crystallization behavior of *i*PP on

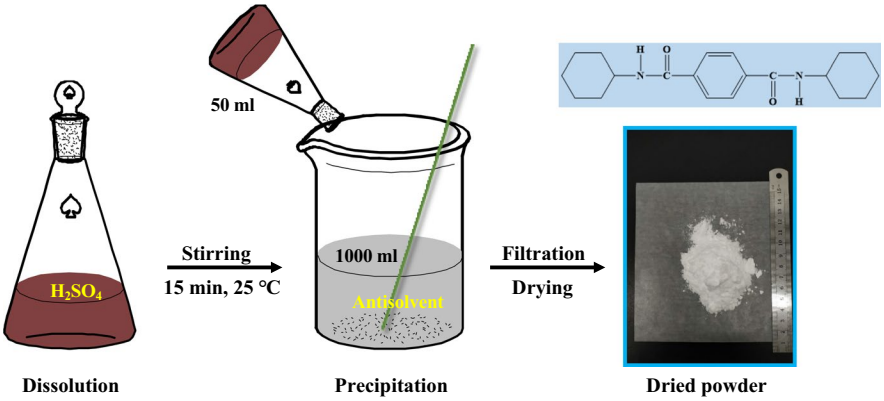

Scheme 1. Preparation of DCHT with different morphologies through antisolvent precipitation method

the DCHT single-crystal surfaces was analyzed in detail. The preparation of DCHT crystals by antisolvent precipitation method provides a new idea for regulating the self-assembly of DCHT. The results of this work can help to understand and further control the crystallization behavior of *i*PP, which has great significance to its practical applications.

Experimental section

Materials and methods

*i*PP with $M_w = 40 \times 10^4$ g/mol and molecular weight distribution of 4.5 was purchased from Lanzhou Petrochemical Company. The β-NA DCHT was supplied by the Shanxi Institute of Chemical Industry.

In order to obtain the DCHT crystals with different morphologies and sizes, commercial DCHT NA was first dissolved in concentrated H_2SO_4 at room temperature (1 g DCHT to 20 ml H_2SO_4). Then the solution was subsequently poured into different antisolvents (H_2O, C_2H_5OH and DMF), and DCHT was precipitated. The ratio of antisolvent to prepared DCHT/H_2SO_4 solution is 20: 1, and the DCHT powder can be almost completely precipitated in the antisolvent at this ratio. After precipitation, the sample was filtered and washed with a large amount of antisolvent until the filtrate was neutral. Finally, the obtained powders were dried for 48 h in a 70 °C oven for use. The DCHT crystals precipitated from each of the antisolvents were, respectively, labeled as DCHT-H_2O, DCHT-C_2H_5OH and DCHT-DMF. The results of Fourier transform infrared (FTIR) and nuclear magnetic resonance (NMR), shown in Fig. S1, indicate that the molecular structure of DCHT has not been destroyed (Scheme 1).

The hybrids containing *i*PP and DCHT were prepared by a Haake PolyLab mixer at 180 °C for 10 min with a rotation speed of 50 rpm. The concentration of DCHT was fixed at 0.1 wt%, and the resulting compound was referred to as *i*PP/0.1DCHT.

Although DCHT is a soluble NA, the dissolution temperature of DCHT varies with concentration [12, 24]. As shown in Fig. S2, the DCHT crystals in the *i*PP/0.1DCHT system could hardly dissolve at 200 °C.

To further investigate the crystal habit and define the crystal parameters of DCHT, a large single crystal with the size of 0.3 mm was also prepared by anti-solvent precipitation method. Firstly, 10 ml readily prepared DCHT H_2SO_4 solution was poured into a Petri dish and sealed with cling film to avoid pollution. After 3 months of growing at room temperature, a rectangular single crystal of DCHT was obtained. The picture of the single crystal is provided in Fig. S3.

Based on the prepared DCHT single crystal, the epitaxial crystallization experiment of *i*PP film was conducted. The *i*PP/xylene solution with a concentration of 1.5 wt% was first prepared at 120 °C; then, the solution was cast on the DCHT single crystal. After the solvent xylene completely evaporated, the crystallization of *i*PP film was observed by Olympus BX 51 microscope with a Linkman hot stage. After eliminating the thermal history at 200 °C, the *i*PP film was quenched to 135 °C and maintained for enough time for complete isothermal crystallization.

Characterization

Scanning electron microscope (SEM)

The SEM (FEI Nova Nano) instrument was used to observe the microscopic morphology of distinct DCHT single-crystal powders and epitaxial crystallization samples. Prior to the observation, the specimens were gold-sputtered.

Differential scanning calorimetry measurement (DSC)

The DSC analysis was conducted on a TA Q20 (USA) instrument under nitrogen purge. The sample weight was about 5.0 mg. In the non-isothermal crystallization process, the temperature was first heated to 200 °C at a rate of 10 °C/min and held for 5 min to eliminate the thermal history. Then the sample was cooled to 40 °C at a rate of 10 °C/min. To observe the melting behavior of *i*PP/0.1DCHT, the sample was then re-heated to 200 °C at a rate of 10 °C/min. During the isothermal crystallization process, the samples were also kept at 200 °C for 5 min to eliminate thermal history and then quenched at 200 °C/min to the target isothermal crystallization temperature [25]. After complete crystallization, the sample was cooled to 40 °C at a rate of 10 °C/min and then heated to 200 °C and its melting behavior was recorded.

X-ray diffraction (XRD)

Single crystal of DCHT (see Fig. S3) was measured by Bruker D8 diffractometer with 0.71073 Å at 296 K. The DCHT crystal structure analysis and refinement were performed by using the SHELXL-97 package.

Powder X-ray diffraction (Ultima IV): copper target, $K_{\alpha l}$ (0.154056 nm), tube voltage 40 kV, tube current 40 mA, 2θ ranging from 5° to 50°, step size 0.02° and time for each step 0.12 s.

Results and discussion

Crystal habit analysis of DCHT

Figure 1a shows the morphologies of commercial DCHT and precipitated DCHT in different antisolvents. Different from the commercial DCHT, the precipitated nucleators DCHT-H_2O, DCHT-DMF and DCHT-C_2H_5OH exhibit particle-like crystallites, cuboid and large rectangular crystals, respectively. In terms of size scale, the commercial and precipitated DCHT can be divided into nanoscale (DCHT-H_2O and DCHT) and microscale (DCHT-DMF and DCHT-C_2H_5OH) crystals. The crystal morphologies obtained by antisolvent method could be influenced by the solubility and intermolecular force [26, 27]. The comparatively smaller crystal size of DCHT-H_2O might be ascribed to the low solubility of DCHT in H_2O. It can be found that the thickness of DCHT-C_2H_5OH is much smaller than that of DCHT-DMF, and the multilayer structure can be observed from the side of DCHT-C_2H_5OH. According to the analysis of DCHT crystal structure by Wang [18], special hydrogen bond structures are speculated to form between C_2H_5OH and DCHT molecules. In order to further analyze the crystal habit of DCHT crystals in different solvents, powder XRD analysis was exhibited in Fig. 1b. The positions of $2\theta = 6.9°$, 17.2°, 19.3° and 21.9° in the figure represent the (002), (100), (014) and (110) planes, respectively. For DCHT-C_2H_5OH, one can see that the (002) diffraction peak is not only the strongest, but also shows the largest contrast with (100) plane, which implies that the DCHT-C_2H_5OH crystal could preferentially grow along the (002) plane. This could further explain the particular large and thin crystal morphology of DCHT-C_2H_5OH, while for the other DCHT crystals, for example DCHT-H_2O, the contrast between (002) plane and (100) plane is not so distinguishable, indicating almost no preferential

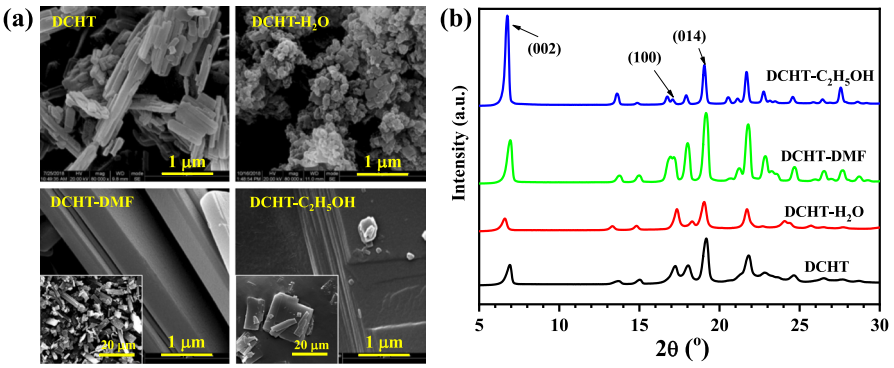

Fig. 1 SEM micrographs (**a**) and XRD curves (**b**) of DCHT with various morphologies

growth plane. Therefore, the XRD results have a good agreement with SEM observation. In addition, the diffraction intensity of the (100) plane is negatively correlated with the size of the different DCHT crystals.

Effect of DCHT crystals on the crystallization behaviors of *i*PP

Figure 2 shows the effect of various DCHT crystals on the crystallization behavior of *i*PP. As displayed in Fig. 2a, the *i*PP/0.1DCHT-H_2O sample exhibited the highest non-isothermal crystallization temperature. These results indicate that DCHT-H_2O has the strongest nucleation ability, which is even better than commercial DCHT. Apparently, this is ascribed to the smallest size (Fig. 1a) or the highest nucleation density. During the melting process (Fig. 2b), the samples containing NA show an obvious β melting peak near 150 °C, which seems to be independent of the DCHT size. Thus, the DCHT size only affects the crystallization rate of *i*PP and has no evident effect on its crystal form at such a non-isothermal process. Then, the isothermal crystallization behavior of *i*PP/0.1DCHT at various temperatures was quantified to assess the effect of different DCHT crystals on the *i*PP crystallization kinetics. As depicted in Fig. 2c and d, two distinct cases were observed in the crystallization rate of *i*PP/0.1DCHT hybrids, with one containing nanoscale NA (*i*PP/0.1DCHT-H_2O

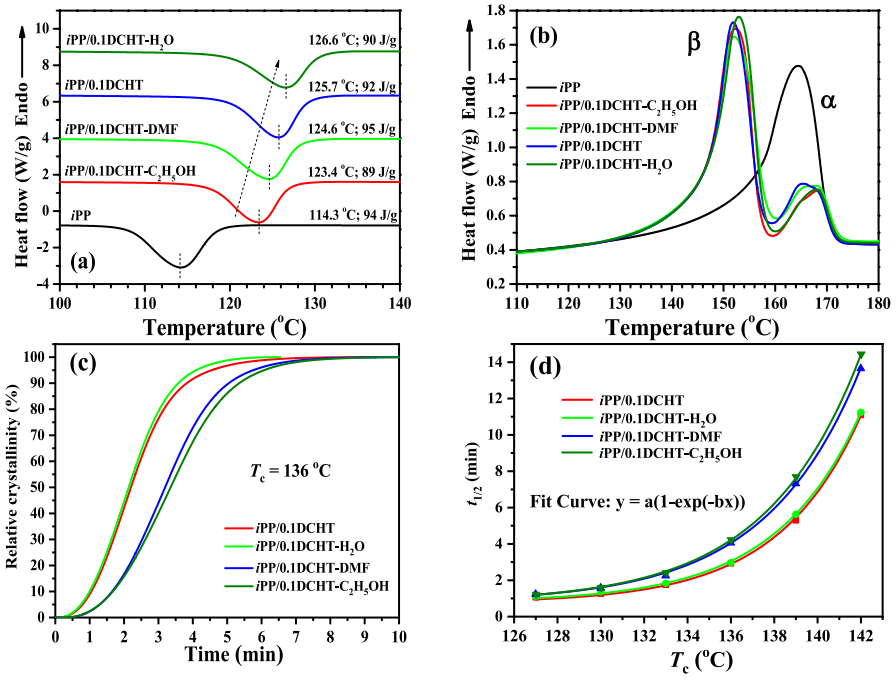

Fig. 2 DSC cooling (**a**) and heating (**b**) scans at a rate of 10 °C/min, the relative crystallinity versus time (**c**) and the half-time of crystallization ($t_{1/2}$) versus crystallization temperature (T_c) (**d**) for *i*PP/0.1DCHT hybrids

and *i*PP/0.1DCHT) and the other containing microscale NA (*i*PP/0.1DCHT-DMF and *i*PP/0.1DCHT-C_2H_5OH). In addition, Fig. 2d illustrates how the changes of half-time of crystallization ($t_{1/2}$) with isothermal crystallization temperature (T_c) for *i*PP/0.1DCHT hybrids and the corresponding exponential fitting curves. This suggests that the crystal growth of *i*PP in this study belongs to three-dimensional heterogeneous growth mode [25].

To further investigate the melting process of *i*PP with different DCHT crystals after isothermal crystallization and the possible phase transitions [28, 29], Fig. 3 shows the DSC melting curves of different *i*PP/0.1DCHT systems after isothermal crystallization at different temperatures. As the isothermal crystallization

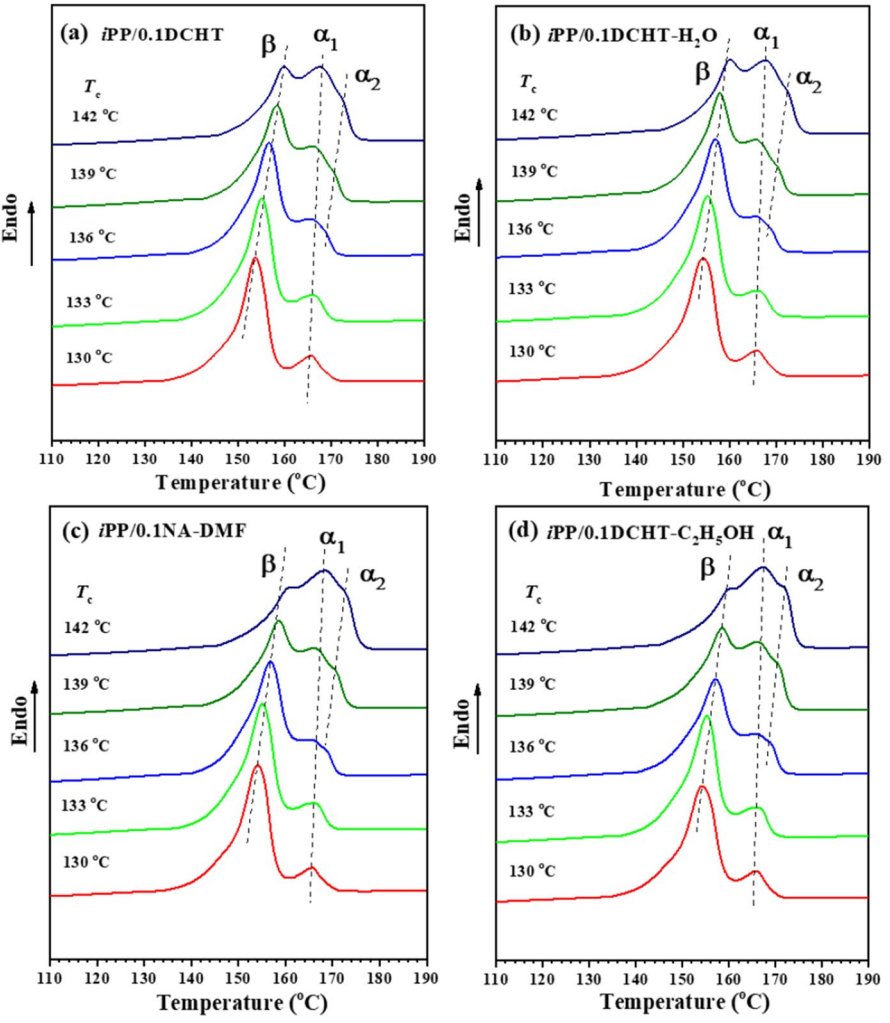

Fig. 3 DSC heating curves after completely isothermal crystallization at different T_c for *i*PP/0.1DCHT hybrids

temperature increases, the melting points of both α and β crystals move to higher temperature due to thicker lamellae [30]. Due to the different thermal history, the α crystal structure often appears different degrees of disorder, and the disorder of this structure is mainly manifested by the different direction of the same spiral chain. The α_1 crystal represents a limit-disordered (space group C2/c) structure, with its spiral chains pointing to complete disorder. Conversely, the α_2 crystal exhibits a limit-ordered (space group $P2_1/c$) structure, with its spiral chains pointing up and down in order. In comparison, α_1 crystals demonstrate a lower degree of order and tend to crystallize at lower temperatures than α_2 crystals [31]. Notably, when the crystallization temperature is 130 °C and 133 °C, no conspicuous α_2 crystal is observed for all samples, which is different the from heating processes at other higher crystallization temperatures. This indicates that *i*PP tends to form α_1 phase with higher disorder in this temperature range [31], which may be attributed to the faster growth kinetics of α_1 phase than α_2 phase [29] and the hard transformation for α_1 to α_2 due to the relatively low temperature. In addition, from 139 to 142 °C, the content of α crystals increases and the content of β crystals decreases. This phenomenon is more obvious in the *i*PP/0.1DCHT-DMF and *i*PP/0.1DCHT-C_2H_5OH systems, where the β crystal melting peak is relatively small. This means that the microscale nucleators (DCHT-DMF and DCHT-C_2H_5OH) are less effective in inducing the formation of β crystals at higher crystallization temperatures. The "β–α growth transition theory" proposed by Varga [32] and Lotz [33] indicates that the growth rate of β crystal is greater than that of α crystal only between 100 and 141 °C. Therefore, *i*PP with the addition of β NA will mainly generate α crystals when the temperature is lower than the lower critical temperature or higher than the upper critical temperature. In the systems (micro- and nanoscale DCHT) studied here, the situations are quite different. In the microscale system, the content of β crystals is significantly lower than that of α crystals at 142 °C, whereas in the nanoscale system, the contents of β and α crystals are almost comparable. This suggests that the α and β growth rate inversion temperature of microscale DCHT system might be lower than that of nanoscale system. Therefore, the upper critical temperature proposed by Varga [32] could be related to the size of NA; that is, a larger size corresponds to a lower upper critical temperature. Understanding these NA dynamics is crucial for comprehending the crystallization process of *i*PP.

As shown in Fig. 4, the XRD patterns of two typical systems containing *i*PP/0.1DCHT-H_2O and *i*PP/0.1DCHT-C_2H_5OH were further analyzed after isothermal crystallization. The characteristic diffraction peaks of pure α-*i*PP and β-*i*PP are resulted from (110), (040), (300), (111), (041) and (110), (300) crystal planes, respectively [34, 35]. As the crystallization temperature increases, the characteristic diffraction peaks (110) and (300) of β phase were found to become progressively shorter. This suggests that the content of β crystals in the two systems gradually decreases, which is consistent with the conclusion drawn in Fig. 3. In addition, the decrease of β crystals in nanoscale DCHT system at high temperature, especially 142 °C, is smaller than that in microscale system with increasing crystallization temperature. This further confirms that the upper critical temperature of the phase transition is indeed related to the size of the NA.

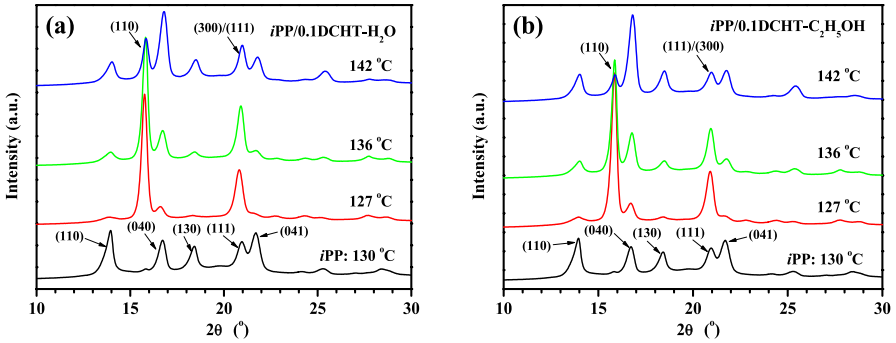

Fig. 4 XRD patterns of *i*PP/0.1DCHT hybrid after completely isothermal crystallization at different T_c (127, 136 and 142 °C) and the pattern of *i*PP (T_c = 130 °C) as a reference

Figure 5 provides an overview of the correlation between the crystallization temperature or crystallization kinetics of *i*PP and the melting points of β and α_1 crystals. As depicted in Fig. 5a, the melting point of β crystals almost develops linearly with the crystallization temperature for all *i*PP/0.1DCHT systems. This is consistent with the H–L theory where lamellar thickness and lamellar surface defects determine the melting point of polymer crystals [36–38]. That is to say, the higher the crystallization temperature, the thicker and more perfect the lamellae will be, ultimately resulting in higher melting point. Unlike the linear change of the $T_{m\beta}$ with increasing crystallization temperature, the melting point of α_1 crystal first increases, then enters a plateau and finally continues to increase. Apparently, there is a phase transition between 133 and 139 °C, which may be caused by the competitive relationship between the growth process of α and β crystals [29].

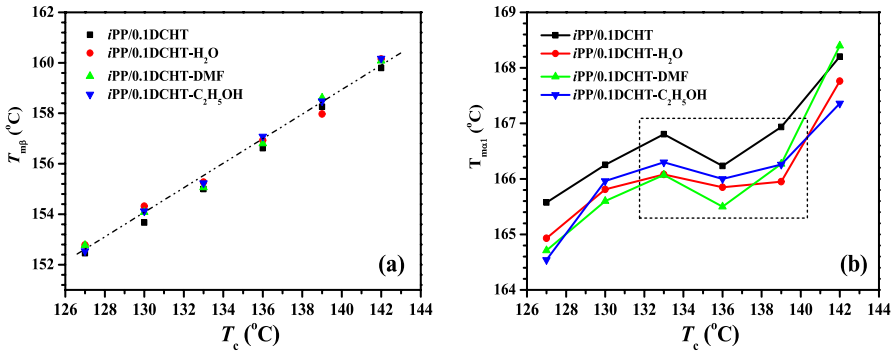

Fig. 5 Dependences of $T_{m\beta}$ versus T_c (**a**) and $T_{m\alpha1}$ versus T_c (**b**) for *i*PP/0.1DCHT hybrids undergone isothermal crystallization

Epitaxial growth of *i*PP on the surface of DCHT crystal

In order to analyze the epitaxial crystallization behavior of iPP on DCHT single-crystal surface, the DCHT single crystals were prepared by the antisolvent method and are shown in Fig. S3. First, single-crystal XRD analysis was performed on the DCHT single crystals. The Crystallographic Information File (CIF) for DCHT crystals can be found at the Cambridge Crystallographic Data Center. The CIF contains detailed information about the crystal, such as cell parameters and atomic coordinates [39]. The collected single-crystal XRD data, along with the CIF, were analyzed using the SHELXL-97 software package, which facilitated the generation of Fig. 6. As shown in Fig. 6, the DCHT crystal is still monoclinic and the unit cell parameters ($a=5.17$ Å, $b=6.65$ Å, $c=25.88$ Å, $\beta=94.52°$, $P2_1/c$) are consistent with the work of Wang's group [18]. This indicates that the antisolvent precipitation method does not change the DCHT unit cell structure. As shown in Fig. 6a–c, analysis of the unit cell from three views reveals that the projection direction of the *a*-axis is consistent with the direction of hydrogen bond formation. Figure 6e shows that the (100) crystal plane corresponds precisely to the plane of DCHT hydrogen bonding. This observation suggests that the growth of the (100) plane could be influenced by the formation of hydrogen bonds [18]. Furthermore, as depicted in Fig. 6f, the minimum distance between the two adjacent DCHT molecules is exactly the

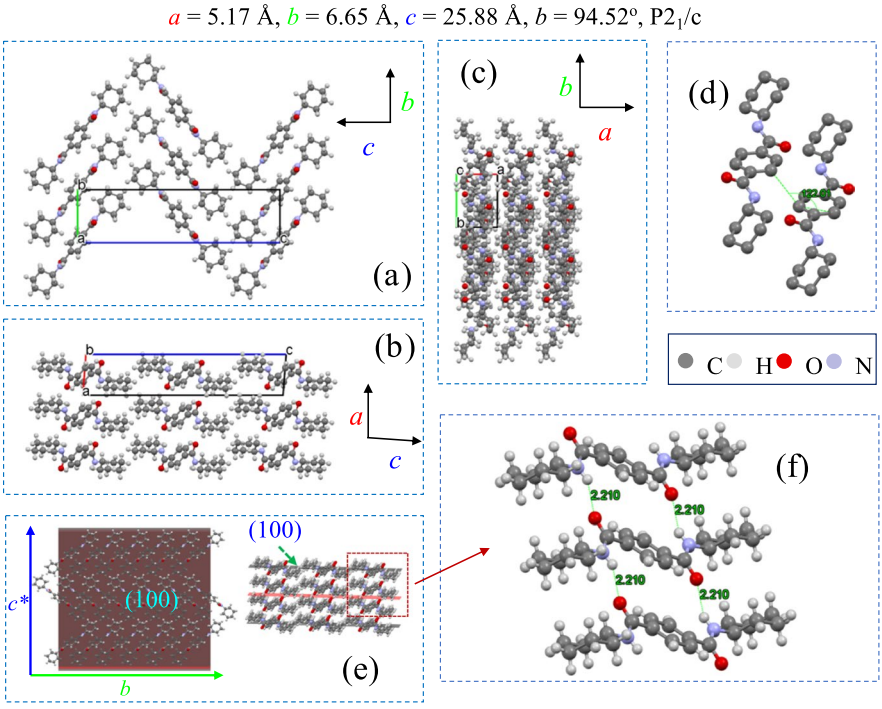

Fig. 6 Molecular structure and packing diagram in DCHT crystal

hydrogen bond distance (2.21 Å), confirming the presence of strong hydrogen bond interactions between DCHT molecules. Combined with the analysis of SEM and XRD results in Fig. 1, the height of the (100) crystal plane is negatively correlated with the size of the DCHT crystal, while the (100) plane is aligned with the hydrogen bonding plane. Therefore, the hydrogen bonding could be the primary driving force for the growth of DCHT crystals. Furthermore, the angle between the edge portions of the benzene rings on two adjacent DCHT molecules is greater than 90° as demonstrated in Fig. 6d, indicating that the DCHT crystal does not contain a π–π stacking structure. This implies that π–π interactions do not influence the stacking of DCHT molecules during the recrystallization process, contrary to the conclusions of Feng's team [12].

To further investigate the crystallization behavior of *i*PP/DCHT, the epitaxy of *i*PP lamellae on the surface of DCHT single crystals was observed by SEM. As shown in Fig. 7a, the long red arrows represent the preferred orientation of DCHT single crystals. It can be clearly seen from the texture with 500 nm resolution that the growth direction of the *i*PP lamellae (20 and 50 nm) is the same as the long-axis direction of the DCHT single crystal. As proved in Fig. 6, the preferred orientation of DCHT is the projection direction of the *a*-axis (the direction of DCHT hydrogen bonding). Since the growth direction of the *i*PP lamellae is perpendicular to the direction of the chain axis of the molecular chain (the molecular chain arrangement is drawn in the 40 μm resolution image), the *c*-axis direction of the β crystal is the same as the direction of the chain axis. Therefore, the *c*-axis direction of the β-*i*PP crystal is perpendicular to the projection direction of the *a*-axis of the DCHT single crystal. Thus, the epitaxial plane of DCHT is the (001) plane, which is consistent with Wang's work [18].

Further, the epitaxial crystallization behavior of *i*PP attached on the surface of DCHT crystal is analyzed from the perspective of lattice matching. Visualized in Fig. 7b is the top view of the DCHT (001) plane, with the *a*-axis projection direction of the DCHT crystal vertically upwards. According to the work of Lotz [17, 40], the contact plane of β-*i*PP during epitaxial crystallization is the (110) plane, and the periodic lattice parameters of the two-dimensional orientation of the (110) crystal plane are the *c*-axis distance of the β crystal (6.5 Å) and the long-axis distance of the rhombic unit cell composed of three independent molecular chains (19.05 Å). Analysis of the DCHT single-crystal data shows that the periodic distance of (001)

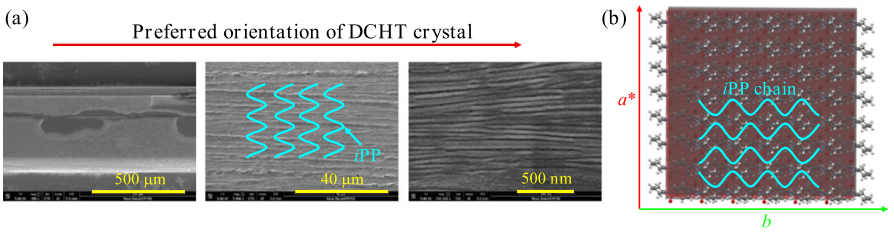

Fig. 7 **a** SEM images for epitaxial crystallization of *i*PP film on DCHT crystal and **b** epitaxial growth of *i*PP chains on DCHT (001) plane

crystal plane in the *b*-axis direction is 6.65 Å. Additionally, the projection length of the *a*-axis (a^*_{DCHT}) on the (001) crystal plane is: $a \times \sin\gamma = 5.17$ Å. Therefore, according to the lattice matching theory [14, 41], the mismatch ratio between the (110) plane of β-*i*PP and the (001) plane of DCHT in the two-dimensional direction is:

$$\frac{c_{\beta\text{ - iPP}} - b_{DCHT}}{b_{DCHT}} \times 100\% = \frac{6.5 - 6.65}{6.65} \times 100\% = -2.26\% \quad (1)$$

$$\frac{D_{\beta\text{ - iPP(110)}} - 4a^*_{DCHT}}{4a^*_{DCHT}} \times 100\% = \frac{19.05 - 4 \times 5.17}{4 \times 5.17} \times 100\% = -7.88\% \quad (2)$$

where $c_{b\text{-ipp}}$, b_{DCHT}, $D_{b\text{-ipp}}$ and a^*_{DCHT} represent the *c*-axis distance of the β-*i*PP unit cell, the *b*-axis distance of the DCHT unit cell, the long-axis distance of the β-*i*PP rhombohedral unit cell and the *a*-axis projection of the DCHT unit cell distance. Obviously, the mismatch ratio of the two crystal planes is smaller than the upper limit (~15%) allowed by the lattice matching theory. This indicates that the (001) plane of the DCHT crystal has a high nucleation density, and theoretically proves that DCHT possesses an excellent inducing β-nucleation ability.

Conclusions

The DCHT crystals with different morphologies were prepared by antisolvent precipitation method, among which DCHT-H_2O appears to be crystallites and DCHT-C_2H_5OH possesses the largest size. The single-crystal XRD results of DCHT single crystal show that there is indeed strong hydrogen bonding among DCHT molecules, and meanwhile, it also suggests that it is impossible to form π–π bonds in DCHT crystal. Combining the powder XRD and SEM, it is found that the diffraction intensity of (100) plane is negatively correlated with the size of the DCHT crystal. In addition, it was found that hydrogen bonds may be the main driving force during the growth of DCHT crystals. Furthermore, the crystallization behavior of *i*PP/DCHT shows that the smaller the size of DCHT, the higher the non-isothermal crystallization temperature of *i*PP, and the higher the upper critical temperature of β-α growth "transition" of *i*PP. Finally, the crystallization behavior of *i*PP/DCHT compounds is analyzed from the lattice match theory further, in which the mismatch rates β-*i*PP and DCHT in the two-dimensional direction are slightly modified: −2.26% and −7.88%.

A number of recommendations for future research are given. For the different DCHT crystal morphologies obtained by the antisolvent method, only some conventional morphologies have been obtained at present, and subsequent studies need to be carried out to further expand the scope of antisolvent aiming to obtain more diverse DCHT morphologies. At the same time, smaller size of DCHT crystals can also be prepared by antisolvent method to improve the crystalization rate of *i*PP, which is helpful for its actual processing applications.

Supplementary Information The online version contains supplementary material available at https://doi.org/10.1007/s00289-024-05254-5.

Acknowledgements Y. H. Niu thanks financial supports from the National Science Foundation of China with grant number 52073184, 51873125. G. X. Li thanks financial support from the National Science Foundation of China with grant number 51721091 and Program of Introducing Talents of Discipline to Universities with grant number B13040.

References

1. Nagarajan K, Levon K, Myerson A (2000) Nucleating agents in polypropylene. J Therm Anal Calorim 59:497–508
2. Varga J, Schulek-Tóth F (1996) Crystallization, melting and spherulitic structure of β-nucleated random propylene copolymers. J Therm Anal Calorim 47:941–955
3. Mao J-J, Jiang Y-Z, Zhou P-Z et al (2020) Nucleus density and crystallization behavior of isotactic polypropylene nucleated with different α/β compound nucleating agents. J Therm Anal Calorim 140:2275–2282
4. Wang J, Ren Z, Sun X et al (2015) The βα growth transition of isotactic polypropylene during stepwise crystallization at elevated temperature. Colloid Polym Sci 293:2823–2830
5. Looijmans S, Menyhard A, Peters GWM et al (2017) Anomalous temperature dependence of isotactic polypropylene α-on-β cross-nucleation kinetics. Cryst Growth Des 17:4936–4943
6. Mohmeyer N, Schmidt H-W, Kristiansen PM et al (2006) Influence of chemical structure and solubility of bisamide additives on the nucleation of isotactic polypropylene and the improvement of its charge storage properties. Macromolecules 39:5760–5767
7. Mencik Z (1972) Crystal structure of isotactic polypropylene. J Macromol Sci Part B 6:101–115
8. Rybnikář F (1991) Transition of β to α phase in isotactic polypropylene. J Macromol Sci Part B 30:201–223
9. Shi S, Liu W, Nie M et al (2016) Localized self-assembly and nucleation: a new strategy for preparing highly toughened polymer blends. RSC Adv 6:98104–98108
10. Chang B, Schneider K, Vogel R et al (2018) Influence of nucleating agent self-assembly on structural evolution of isotactic polypropylene during uniaxial stretching. Polymer 138:329–342
11. Liu L, Zhao Y, Zhang C et al (2021) Morphological characteristics of β-nucleating agents governing the formation of the crystalline structure of isotactic polypropylene. Macromolecules 54:6824–6834
12. Yue Y, Yi J, Wang L et al (2020) Toward a more comprehensive understanding on the structure evolution and assembly formation of a bisamide nucleating agent in polypropylene melt. Macromolecules 53:4381–4394
13. Hu D, Wang G, Feng J et al (2016) Exploring supramolecular self-assembly of a bisamide nucleating agent in polypropylene melt: the roles of hydrogen bond and molecular conformation. Polymer 93:123–131
14. Wittmann JC, Lotz B (1981) Epitaxial crystallization of polyethylene on organic substrates: a reappraisal of the mode of action of selected nucleating agents. J Polym Sci Polym Phys Ed 19:1837–1851
15. Lotz B, Miyoshi T, Cheng SZ (2017) 50th anniversary perspective: polymer crystals and crystallization: personal journeys in a challenging research field. Macromolecules 50:5995–6025
16. Sun Y, Zhao S, Zhang X et al (2020) Structural relationships between zinc hexahydrophthalate and the β phase of isotactic polypropylene. Ind Eng Chem Res 59:18529–18538
17. Stocker W, Schumacher M, Graff S et al (1998) Epitaxial crystallization and AFM investigation of a frustrated polymer structure: isotactic poly (propylene), β phase. Macromolecules 31:807–814
18. Wang Z, Yang W, Liu G et al (2017) Probing into the epitaxial crystallization of β form isotactic polypropylene: from experimental observations to molecular mechanics computation. J Polym Sci Part B Polym Phys 55:418–424
19. Zhu P, Song F, Ma P et al (2016) Morphology-controlled self-assembly of a ferrocene–porphyrin based NO_2 gas sensor: tuning the semiconducting nature via solvent–solute interaction. J Mater Chem C 4:10471–10478

20. Thorat AA, Dalvi SV (2012) Liquid antisolvent precipitation and stabilization of nanoparticles of poorly water soluble drugs in aqueous suspensions: recent developments and future perspective. Chem Eng J 181:1–34
21. D'addio SM, Prud'homme RK (2011) Controlling drug nanoparticle formation by rapid precipitation. Adv Drug Deliv Rev 63:417–426
22. Algra RE, Graswinckel WS, Van Enckevort WJP et al (2005) Alizarin crystals: an extreme case of solvent induced morphology change. J Cryst Growth 285:168–177
23. Millan A (2000) New method for the production of silver halide tabular crystals. J Cryst Growth 208:592–598
24. Luo G, Zhang B, Gong P et al (2021) Reexamination of self-assembly of nucleator and its influence on the crystallization of polypropylene. Polymer 231:124139
25. Zhang YF, Xin Z (2007) Isothermal crystallization behaviors of isotactic polypropylene nucleated with α/β compounding nucleating agents. J Polym Sci Part B Polym Phys 45:590–596
26. Takiyama H, Minamisono T, Osada Y et al (2010) Operation design for controlling polymorphism in the anti-solvent crystallization by using ternary phase diagram. Chem Eng Res Des 88:1242–1247
27. Chai S, Li E, Zhang L et al (2022) Crystallization solvent design based on a new quantitative prediction model of crystal morphology. AIChE J 68:e17499
28. Lovinger AJ, Chua JO, Gryte CC (1977) Studies on the α and β forms of isotactic polypropylene by crystallization in a temperature gradient. J Polym Sci Polym Phys Ed 15:641–656
29. Nakamura K, Shimizu S, Umemoto S et al (2008) Temperature dependence of crystal growth rate for α and β forms of isotactic polypropylene. Polym J 40:915–922
30. Iijima M, Strobl G (2000) Isothermal crystallization and melting of isotactic polypropylene analyzed by time- and temperature-dependent small-angle X-ray scattering experiments. Macromolecules 33:5204–5214
31. Auriemma F, De Ballesteros OR, De Rosa C et al (2000) Structural disorder in the α form of isotactic polypropylene. Macromolecules 33:8764–8774
32. Varga J (1989) β-Modification of polypropylene and its two-component systems. J Therm Anal 35:1891–1912
33. Lotz B (1998) α and β phases of isotactic polypropylene: a case of growth kineticsphase reentrency'in polymer crystallization. Polymer 39:4561–4567
34. Mathieu C, Thierry A, Wittmann J et al (2000) "Multiple" nucleation of the (010) contact face of isotactic polypropylene, α phase. Polymer 41:7241–7253
35. Luo F, Geng C, Wang K et al (2009) New understanding in tuning toughness of β-polypropylene: the role of β-nucleated crystalline morphology. Macromolecules 42:9325–9331
36. Hoffman JD, Lauritzen JI Jr (1961) Crystallization of bulk polymers with chain folding: theory of growth of lamellar spherulites. J Res Natl Bur Stand Sect A Phys Chem 65:297
37. Hoffman JD, Davis GT, Lauritzen JI (1976) The rate of crystallization of linear polymers with chain folding. In: Hannay NB (ed) Treatise on solid state chemistry. Springer, Belrin, pp 497–614
38. Cheng SZD, Lotz B (2005) Enthalpic and entropic origins of nucleation barriers during polymer crystallization: the Hoffman–Lauritzen theory and beyond. Polymer 46:8662–8681
39. Mcmahon (2006) The crystallographic information file (CIF). Data Sci J 5:174–177
40. Mathieu C, Thierry A, Wittmann JC et al (2002) Specificity and versatility of nucleating agents toward isotactic polypropylene crystal phases. J Polym Sci Part B Polym Phys 40:2504–2515
41. Wittmann JC, Lotz B (1990) Epitaxial crystallization of polymers on organic and polymeric substrates. Prog Polym Sci 15:909–948